

Nuclear mean field from chiral pion-nucleon dynamics¹

N. Kaiser^a, S. Fritsch^a and W. Weise^{a,b}

^a Physik Department, Technische Universität München, D-85747 Garching, Germany

^b ECT*, I-38050 Villazzano (Trento), Italy

email: nkaiser@physik.tu-muenchen.de

Abstract

Using the two-loop approximation of chiral perturbation theory, we calculate the momentum and density dependent single particle potential of nucleons in isospin-symmetric nuclear matter. The contributions from one- and two-pion exchange diagrams give rise to a potential depth for a nucleon at rest of $U(0, k_{f0}) = -53.2 \text{ MeV}$ at saturation density. The momentum dependence of the real part of the single particle potential $U(p, k_{f0})$ is non-monotonic and can be translated into a mean effective nucleon mass of $\bar{M}^* \simeq 0.8M$. The imaginary part of the single particle potential $W(p, k_f)$ is generated to that order entirely by iterated one-pion exchange. The resulting half width of a nucleon hole-state at the bottom of the Fermi sea comes out as $W(0, k_{f0}) = 29.7 \text{ MeV}$. The basic theorems of Hugenholtz-Van-Hove and Luttinger are satisfied in our perturbative two-loop calculation of the nuclear mean field.

PACS: 12.38.Bx, 21.65.+f

Keywords: Effective field theory at finite density, Real and imaginary part of the single particle potential in nuclear matter, effective nucleon mass.

1 Introduction and summary

The shell model and the optical model have always played a central role in the description of nuclear structure and nuclear reactions. The knowledge of single particle properties in dense nuclear matter is therefore of basic importance for the understanding of both nuclear structure and nuclear dynamics. Quantities like the nuclear mean field (or equivalently the single particle potential), the nucleon mean free path, the effective mass, etc., enter in the description of static as well as dynamic properties of nuclei (for a review see ref.[1]). Considerable progress has been made during the past decades in calculating these single particle quantities from first principles, based on non-relativistic Brueckner theory [2, 3] and relativistic many-body theory [4, 5]. Despite the widely different mechanisms which build up the nuclear mean field in these two theoretical approaches, the depth of the single particle potential comes out at approximately the same value when both calculations are restricted to first order in the renormalized in-medium NN-interaction

¹ Work supported in part by BMBF, GSI and DFG.

(G-matrix). Other properties, such as the momentum dependence of the nuclear mean field are also qualitatively similar in those two approaches.

In a recent work [6], we have used chiral perturbation theory for a systematic treatment of the nuclear matter many-body problem. In this calculation the contributions to the energy per particle, $\bar{E}(k_f)$, originate exclusively from one- and two-pion exchange between nucleons and they are ordered in powers of the Fermi momentum k_f (modulo functions of k_f/m_π with m_π denoting the pion mass). It has been demonstrated in ref.[6] that the empirical saturation point and the nuclear matter compressibility $K \simeq 250$ MeV can be well reproduced at order $\mathcal{O}(k_f^5)$ in the chiral expansion with just one single momentum cut-off scale of $\Lambda \simeq 0.65$ GeV which parametrizes all necessary short range dynamics. Most surprisingly, the prediction for the asymmetry energy, $A_0 = 33.8$ MeV, is in very good agreement with its empirical value. Furthermore, as a nontrivial fact pure neutron matter is predicted to be unbound and the corresponding equation of state agrees roughly with that of sophisticated many body calculations for low neutron densities $\rho_n \leq 0.25$ fm $^{-3}$.

Given the fact that the bulk properties of nuclear matter can be well described by chiral pion-nucleon dynamics treated up to three loop order it is natural to consider in a next step quantities which characterize in more detail the behavior of a single nucleon moving in the dense nuclear matter environment. It is the purpose of this work to calculate, using the same framework as in ref.[6], the momentum and density dependent (complex-valued) single particle potential of nucleons in isospin-symmetric nuclear matter. We will present here analytical expressions for both the real part $U(p, k_f)$ and the imaginary part $W(p, k_f)$ of the nuclear mean field generated by chiral one- and two-pion exchange. Our results can be summarized as follows:

- i) At equilibrium nuclear matter density chiral one- and two-pion exchange generate an attractive nuclear mean field for nucleons at rest, with a depth of $U(0, k_{f0}) = -53.2$ MeV. This value is in very good agreement with the depth of the empirical optical model potential $U_0 \simeq -52$ MeV deduced by extrapolation from elastic nucleon-nucleus scattering data [7, 8]. In fact, the average nuclear potential employed in shell model calculations of nuclei has approximately the same depth [9].
- ii) The momentum dependence of the real part of the single particle potential $U(p, k_{f0})$ is non-monotonic in the momentum interval $0 \leq p \leq k_{f0}$. Its maximal increase of $\Delta U = 8.8$ MeV can be translated into an average effective nucleon mass of $\bar{M}^* = 0.82M$. This is comparable to the empirical value of the effective nucleon mass in nuclear matter, $M_{emp}^* = (0.7 - 0.8)M$, derived from experimental data in the framework of non-relativistic shell or optical models [10, 11, 12].
- iii) To the order considered here the imaginary part of the single particle potential $W(p, k_f)$ is entirely generated by iterated one-pion exchange. For a nucleon hole-state at the bottom of the Fermi sea, one finds a half width $\Gamma_{hole}/2 = W(0, k_{f0}) = 29.7$ MeV. This value is not far from results obtained in Brueckner-Hartree-Fock calculations based on realistic NN-forces, where $W(0, k_{f0}) \simeq 40$ MeV [3].
- iv) The Hugenholtz-Van-Hove theorem [13] which relates the total single particle energy at the Fermi surface (i.e. the Fermi energy) to the nuclear matter equation of state is satisfied in our two-loop chiral perturbation theory calculation. Luttinger's theorem [14] does also hold since the calculated imaginary part, $W(p, k_f) \sim (k_f - p)^2$, vanishes quadratically near the Fermi surface. The associated curvature coefficient $C(k_f)$ grows with density approximately as $\rho^{2/3}$.

As a combined conclusion of ref.[6] and this work one can thus state that perturbative chiral pion nucleon dynamics gives realistic nuclear binding and saturation as well as realistic (in-medium) single particle properties.

2 Single particle potential of nucleons in nuclear matter

The nuclear mean field (or single particle potential) is generally defined through the momentum and density dependent nucleon self energy in (isospin symmetric) nuclear matter. In a diagrammatic calculation this quantity is derived from the in-medium nucleon propagator taking into account interactions among nucleons up to a certain order as well as Pauli-blocking effects. On the other hand, the ground state energy density of nuclear matter is represented diagrammatically by analogous closed vacuum graphs which result from closing the nucleon line of a self energy diagram. As outlined in section 2 of ref.[6] the diagrammatic calculation of the ground state energy density can be organized in the number of so-called medium insertions. The latter is a technical notation for the difference between the vacuum and the bare in-medium nucleon propagator. Let us consider the structure of the energy density according to such an ordering scheme [6]. It consists of a sum of convolution integrals of the form,

$$\begin{aligned} \mathcal{E}[d] = & \int d^3p_1 \mathcal{K}_1 d(\vec{p}_1) + \int d^3p_1 d^3p_2 \mathcal{K}_2 d(\vec{p}_1) d(\vec{p}_2) + \int d^3p_1 d^3p_2 d^3p_3 \mathcal{K}_3 d(\vec{p}_1) d(\vec{p}_2) d(\vec{p}_3) \\ & + \int d^3p_1 d^3p_2 d^3p_3 d^3p_4 \mathcal{K}_4 d(\vec{p}_1) d(\vec{p}_2) d(\vec{p}_3) d(\vec{p}_4). \end{aligned} \quad (1)$$

The one-body kernel $\mathcal{K}_1 = 4T_k(|\vec{p}_1|)$ is four times the relativistically improved kinetic energy (see eq.(3)). $\mathcal{K}_{2,3}$ are two- and three-body kernels related to contributions of closed diagrams with two and three medium insertions. In three-loop approximation the four-body kernel \mathcal{K}_4 is proportional to $\delta^3(\vec{p}_1 + \vec{p}_2 + \vec{p}_3 + \vec{p}_4)$ and purely imaginary. The quantity $d(\vec{p}_j)$ denotes the density of states in momentum space. Inserting the density of states of a filled Fermi sea, $d(\vec{p}_j) = (2\pi)^{-3} \theta(k_f - |\vec{p}_j|)$, into eq.(1) one gets the energy density of nuclear matter, $\rho \bar{E}(k_f)$, with the nucleon density $\rho = 2k_f^3/3\pi^2$. The single particle potential can now be directly constructed from the energy density functional eq.(1) by adding a test nucleon of fixed momentum \vec{p} to the filled Fermi sea. This situation is described by the density of states $d(\vec{p}_j) = (2\pi)^{-3} \theta(k_f - |\vec{p}_j|) + \eta \delta^3(\vec{p} - \vec{p}_j)$ with the infinitesimal parameter η to be interpreted as (\pm) the inverse (infinite) volume. The plus sign applies for a particle ($|\vec{p}| > k_f$) and the minus sign for a hole ($|\vec{p}| < k_f$). Inserting this density of states into eq.(1) leads to

$$\mathcal{E} = \rho \bar{E}(k_f) + 4\eta \left\{ T_k(p) + U(p, k_f) + i W(p, k_f) \right\}, \quad (2)$$

with

$$T_k(p) = \frac{p^2}{2M} - \frac{p^4}{8M^3}, \quad (3)$$

the relativistically improved kinetic energy. The factor 4 in eq.(2) simply counts the spin- and isospin multiplicity of a nucleon. The real and imaginary parts of the single particle potential have, according to eq.(1), a decomposition into two-, three- and four-body contributions,

$$U(p, k_f) = U_2(p, k_f) + U_3(p, k_f), \quad W(p, k_f) = W_2(p, k_f) + W_3(p, k_f) + W_4(p, k_f), \quad (4)$$

where the index on each term refers to the corresponding kernel \mathcal{K}_n in eq.(1). The energy per particle $\bar{E}(k_f)$ in symmetric nuclear matter can also be reconstructed from these components of

the single particle potential by integrating over a Fermi-sphere of radius k_f ,

$$\bar{E}(k_f) = \frac{3}{k_f^3} \int_0^{k_f} dp p^2 \left[T_k(p) + \frac{1}{2} U_2(p, k_f) + \frac{1}{3} U_3(p, k_f) \right]. \quad (5)$$

Note the weighting factors $1/2$ and $1/3$. These take care of combinatoric factors and the fact that three topologically equivalent closed vacuum diagrams with three medium insertions are generated by closing the nucleon line of a self energy diagram. Since this closing procedure must lead to a real energy per particle $\bar{E}(k_f)$ the components of the imaginary part of the single particle potential have to fulfill the zero sum rule

$$\frac{3}{k_f^3} \int_0^{k_f} dp p^2 \left[\frac{1}{2} W_2(p, k_f) + \frac{1}{3} W_3(p, k_f) + \frac{1}{4} W_4(p, k_f) \right] = 0. \quad (6)$$

A further constraint on the single particle potential is given by the Hugenholtz-van-Hove theorem [13]. It states that the total single particle energy at the Fermi surface, $p = k_f$, (i.e. the Fermi energy) is equal to the chemical potential. According to a general thermodynamic relation this chemical potential is the derivative of the energy density $\rho \bar{E}(k_f)$ with respect to the particle density ρ . The Hugenholtz-van-Hove theorem reads explicitly,

$$T_k(k_f) + U(k_f, k_f) = \bar{E}(k_f) + \frac{k_f}{3} \frac{\partial \bar{E}(k_f)}{\partial k_f}, \quad W(k_f, k_f) = 0. \quad (7)$$

Note that the derivative term $\partial \bar{E}(k_f) / \partial k_f$ vanishes at nuclear matter saturation density and therefore the Fermi energy of equilibrated nuclear matter is equal to the negative average binding energy per particle, $\bar{E}(k_{f0})$. Eqs.(5,6,7) serve as important numerical and analytical checks on our chiral perturbation theory calculation to be presented in the next two sections.

3 Real part of the single particle potential

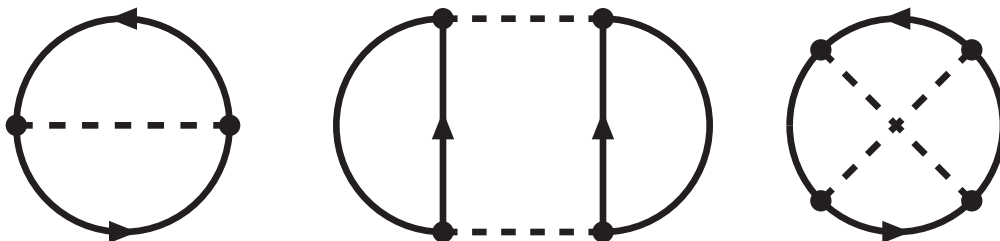


Fig. 1: One-pion exchange Fock-diagram and iterated one-pion exchange Hartree- and Fock-diagrams. The combinatoric factor of these diagrams are $1/2$, $1/4$ and $1/4$, in the order shown. Each nucleon propagator consists of a vacuum part and a medium insertion.

In this section we present analytical results for the real part of the single particle potential $U(p, k_f)$ as given by chiral one- and two-pion exchange. The closed vacuum diagrams related to one-pion exchange (Fock-diagram) and iterated one-pion exchange (Hartree- and Fock-diagrams) are shown in Fig. 1. Each nucleon propagator consists of a vacuum part and a medium insertion (for details see eq.(3) in ref.[6]). Self energy diagrams are obtained from these closed graphs by opening one nucleon line with a medium insertion. In order to keep their number small and in

order to avoid repetitions we associate the contributions to the (real) nuclear mean field $U(p, k_f)$ with the closed vacuum diagram before opening of a nucleon line. The index n on $U_n(p, k_f)$ (see eq.(4)) then indicates the number of medium insertions of the closed vacuum diagram before line opening. From a technical point of view, the calculation of a contribution $U_n(p, k_f)$ (or $W_n(p, k_f)$) involves an integral over the product of $n - 1$ Fermi spheres of radius k_f .

We start with the 1π -exchange Fock-diagram in Fig. 1 with two medium insertions. With inclusion of the relativistic $1/M^2$ -correction one finds a density and momentum dependent real two-body potential of the form,

$$\begin{aligned}
U_2(p, k_f) = & \frac{3g_A^2 m_\pi^3}{(4\pi f_\pi)^2} \left\{ \frac{2u^3}{3} - u + \arctan(u+x) + \arctan(u-x) + \frac{x^2 - u^2 - 1}{4x} \ln \frac{1 + (u+x)^2}{1 + (u-x)^2} \right. \\
& + \frac{m_\pi^2}{16M^2} \left[4u \left(1 - \frac{u^2}{3} - \frac{4u^4}{5} + 3x^2 - \frac{4}{3}u^2x^2 \right) - (2 + 8x^2) \left[\arctan(u+x) \right. \right. \\
& \left. \left. + \arctan(u-x) \right] + \frac{1}{x}(u^2 - x^2)(u^2 + 3x^2) \ln \frac{1 + (u+x)^2}{1 + (u-x)^2} \right] \left. \right\}, \quad (8)
\end{aligned}$$

where we have introduced the abbreviations $u = k_f/m_\pi$ and $x = p/m_\pi$. As in ref.[6], we choose the value $g_A = 1.3$ for the nucleon axial vector coupling constant. $f_\pi = 92.4$ MeV denotes the weak pion decay constant and $m_\pi = 135$ MeV stands for the (neutral) pion mass. The iterated 1π -exchange Hartree-diagram (second graph in Fig. 1) with two medium insertions gives rise to a real part of the single particle potential which reads

$$\begin{aligned}
U_2(p, k_f) = & \frac{g_A^4 M m_\pi^4}{(4\pi)^3 f_\pi^4} \left\{ \left(\frac{9}{2} + 3u^2 + \frac{2u^3}{x} - x^2 \right) \arctan(u+x) + \left(\frac{9}{2} + 3u^2 - \frac{2u^3}{x} - x^2 \right) \right. \\
& \left. \times \arctan(u-x) - \frac{11u}{2} + \frac{1}{8x}(15x^2 - 15u^2 - 7) \ln \frac{1 + (u+x)^2}{1 + (u-x)^2} \right\}. \quad (9)
\end{aligned}$$

In this expression we have omitted the contribution of a linear divergence proportional to the cut-off Λ (see ref.[6]). All such powerlike terms in Λ are collected in eq.(17). The iterated 1π -exchange Fock-diagram (third graph in Fig. 1) with two medium insertions gives rise to a further contribution to the two-body potential $U_2(p, k_f)$ of the form,

$$\begin{aligned}
U_2(p, k_f) = & \frac{g_A^4 M m_\pi^4}{(4\pi)^3 f_\pi^4} \left\{ u^3 + \left[\int_0^{(u-x)/2} d\xi 2\xi + \int_{(u-x)/2}^{(u+x)/2} d\xi \frac{1}{4x}(u^2 - (2\xi - x)^2) \right] \right. \\
& \left. \times \frac{3}{1 + 2\xi^2} \left[(1 + 8\xi^2 + 8\xi^4) \arctan \xi - (1 + 4\xi^2) \arctan 2\xi \right] \right\}, \quad (10)
\end{aligned}$$

where we have again transferred a term linear in the cut-off Λ to eq.(17). The notation in eq.(10) is to be understood such that the factor in the second line belongs to both integrals. Next, we consider the iterated 1π -exchange Hartree-diagram (second graph in Fig. 1) with three medium insertions. In this case one gets three different contributions to the three-body potential $U_3(p, k_f)$ corresponding to the three possibilities of opening a nucleon line. Altogether they read,

$$\begin{aligned}
U_3(p, k_f) = & \frac{6g_A^4 M m_\pi^4}{(4\pi f_\pi)^4} \int_{-1}^1 dy \left\{ \left[2uxy + (u^2 - x^2y^2) \ln \frac{u+xy}{u-xy} \right] \left[\frac{2s^2 + s^4}{2(1+s^2)} - \ln(1+s^2) \right] \right. \\
& + \int_{-xy}^{s-xy} d\xi \left[2u\xi + (u^2 - \xi^2) \ln \frac{u+\xi}{u-\xi} \right] \frac{(xy+\xi)^5}{[1+(xy+\xi)^2]^2} \\
& \left. + \int_0^u d\xi \frac{\xi^2}{x} \ln \frac{|x+\xi y|}{|x-\xi y|} \left[\frac{2\sigma^2 + \sigma^4}{1+\sigma^2} - 2 \ln(1+\sigma^2) \right] \right\}, \quad (11)
\end{aligned}$$

with the auxiliary functions,

$$s = xy + \sqrt{u^2 - x^2 + x^2y^2}, \quad \sigma = \xi y + \sqrt{u^2 - \xi^2 + \xi^2y^2}. \quad (12)$$

Note that the expressions in eq.(11) originate from a six-dimensional principal value integral over the product of two Fermi spheres of radius k_f . The actual integrands have simple poles located on a five-dimensional quadratic hypersurface. The same features hold for the iterated 1π -exchange Fock-diagram (third graph in Fig. 1) with three medium insertions. Its contribution to the three-body potential $U_3(p, k_f)$ reads

$$\begin{aligned} U_3(p, k_f) = & \frac{3g_A^4 M m_\pi^4}{(4\pi f_\pi)^4} \left\{ \frac{G^2(x)}{8x^2} + \int_0^u d\xi G(\xi) \left[1 + \frac{\xi^2 - x^2 - 1}{4x\xi} \ln \frac{1 + (x + \xi)^2}{1 + (x - \xi)^2} \right] \right. \\ & + \int_{-1}^1 dy \left[\int_{-1}^1 dz \frac{yz \theta(y^2 + z^2 - 1)}{4|yz|\sqrt{y^2 + z^2 - 1}} [s^2 - \ln(1 + s^2)] [\ln(1 + t^2) - t^2] \right. \\ & + \int_0^u d\xi \frac{\xi^2}{x} [\ln(1 + \sigma^2) - \sigma^2] \left(\ln \frac{|x + \xi y|}{|x - \xi y|} \right. \\ & \left. \left. + \frac{1}{R} \ln \frac{[xR + (x^2 - \xi^2 - 1)y\xi]^2}{[1 + (x + \xi)^2][1 + (x - \xi)^2]|x^2 - \xi^2y^2|} \right) \right] \left. \right\}, \quad (13) \end{aligned}$$

where we have introduced some new auxiliary functions,

$$G(x) = u(1 + u^2 + x^2) - \frac{1}{4x} [1 + (u + x)^2][1 + (u - x)^2] \ln \frac{1 + (u + x)^2}{1 + (u - x)^2}, \quad (14)$$

$$t = xz + \sqrt{u^2 - x^2 + x^2z^2}, \quad R = \sqrt{(1 + x^2 - \xi^2)^2 + 4\xi^2(1 - y^2)}. \quad (15)$$

Note that all terms from iterated 1π -exchange are proportional to the (large) nucleon mass, $M = 939$ MeV. The additional diagrams of irreducible 2π -exchange (not shown here, but see Fig. 4 in ref.[6]) with two medium insertions lead to a real single particle potential which can be written as,

$$\begin{aligned} U_2(p, k_f) = & \frac{m_\pi^5}{(4\pi f_\pi)^4} \left[\int_0^{(u-x)/2} d\xi 8\xi + \int_{(u-x)/2}^{(u+x)/2} d\xi \frac{1}{x} (u^2 - (2\xi - x)^2) \right] \left\{ \frac{4}{\sqrt{1 + \xi^2}} \ln(\xi + \sqrt{1 + \xi^2}) \right. \\ & \times [g_A^4(11\xi^4 + 16\xi^2 + 8) - 2g_A^2(5\xi^4 + 7\xi^2 + 2) - (1 + \xi^2)^2] + (1 - 14g_A^2 + 61g_A^4)\xi \\ & \left. + 2(1 + 2g_A^2 + 5g_A^4)\xi^3 + [6(15g_A^4 - 6g_A^2 - 1)\xi + 4(11g_A^4 - 10g_A^2 - 1)\xi^3] \ln \frac{m_\pi}{2\Lambda} \right\} \quad (16) \end{aligned}$$

In order to avoid very lengthy analytical expressions we have stayed at a one-parameter integral representation in eq.(16).

Finally, we give the complete expression for the power divergences specific to cut-off regularization,

$$U_2(p, k_f) = \frac{2\Lambda k_f^3}{(4\pi f_\pi)^4} \left[-10g_A^4 M + (3g_A^2 + 1)(g_A^2 - 1)\Lambda \right]. \quad (17)$$

The term linear in the cut-off Λ stems from iterated 1π -exchange with a contribution of the Hartree- and Fock diagram in the ratio 4 : 1. The term quadratic in the cut-off, on the other hand, originates from irreducible 2π -exchange. Note that the momentum independent contribution to the two-body potential $U_2(p, k_f)$ in eq.(17) is just twice its contribution to the energy per particle $\bar{E}(k_f)$. This relative factor of 2 is typical for a momentum independent NN-contact interaction, to which the power divergences are completely equivalent, as emphasized in ref.[6].

3.1 Results

For the numerical evaluation of the real single particle potential $U(p, k_f)$ we use consistently the same parameters as in our previous work [6]. There, the cut-off scale $\Lambda = 646.3$ MeV has been fine-tuned to the binding energy per particle, $-\bar{E}(k_{f0}) = 15.26$ MeV. With this input the prediction for nuclear matter saturation density was $\rho_0 = 0.178$ fm $^{-3}$ (corresponding to a Fermi momentum of $k_{f0} = 272.7$ MeV) and the nuclear compressibility came out as $K = 255$ MeV.

In Fig. 2, we show the total real single particle potential $U(0, k_f)$ of our calculation for a nucleon at rest ($p = 0$) as a function of the nucleon density $\rho = 2k_f^3/3\pi^2$. The shape of the curve in Fig. 2 is very similar to the nuclear matter equation of state (the so-called saturation curve). In comparison to the energy per particle, $\bar{E}(k_f)$, the scale on the ordinate is stretched by a factor of about 3.5. Interestingly, the potential depth $U(0, k_f)$ reaches its minimum close to the saturation density $\rho_0 = 0.178$ fm $^{-3}$. The actual value at that point is $U(0, k_{f0}) = -53.2$ MeV. This value is in good agreement with the depth of the empirical optical model potential $U_0 \simeq -52$ MeV deduced by extrapolation from elastic nucleon-nucleus scattering data [7, 8]. The average nuclear potential used as input in shell model calculations of nuclei has approximately the same depth (see section 2.4 in ref.[9]). For comparison, the calculation of ref.[3] based on the phenomenological Paris NN-potential finds a potential depth of $U(0, k_{f0}) \simeq -64$ MeV. In the relativistic Dirac-Brueckner approach of ref.[5] using the Bonn-A NN-potential a somewhat deeper real single particle potential with $U(0, k_{f0}) \simeq -80$ MeV has been found. It should also be noted that the potential depth obtained in the present work results from a cancelation of individually large attractive and repulsive terms. For example, when ordering the contributions to $U(0, k_{f0})$ in third, fourth and fifth power of small momenta one has $U(0, k_{f0}) = (-314.7 + 277.4 - 15.9)$ MeV. The decomposition of the same number into contributions from 1π -exchange, iterated 1π -exchange and irreducible 2π -exchange reads $U(0, k_{f0}) = (33.0 - 109.3 + 23.1)$ MeV. Similar features hold also for the binding energy per particle $-\bar{E}(k_{f0}) = 15.26$ MeV (see the discussion in section 2.5 of ref.[6]).

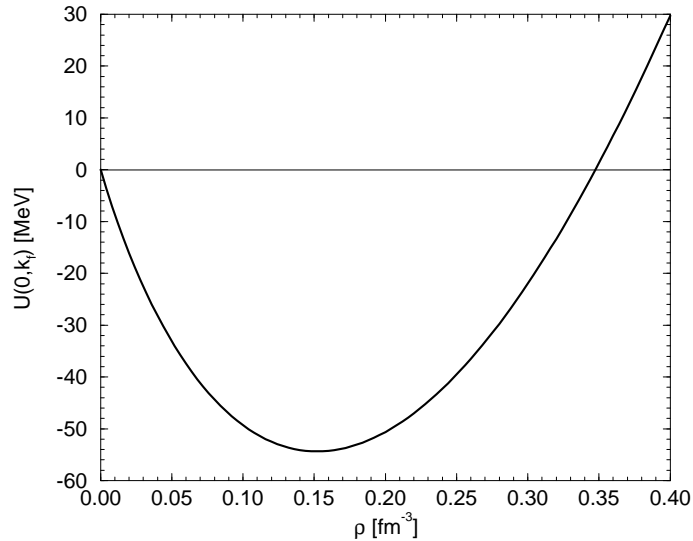


Fig. 2: The real part of the single particle potential $U(0, k_f)$ at nucleon momentum $p = 0$ versus the density $\rho = 2k_f^3/3\pi^2$.

We note that both the sum rule eq.(5) and the Hugenholtz-van-Hove theorem eq.(7) hold with very high numerical accuracy in our calculation. The validity of the Hugenholtz-van-Hove theorem eq.(7) can easily be proven in the present framework on the basis of the density of states $d(\vec{p}_j) = (2\pi)^{-3} \theta(k_f - |\vec{p}_j|) + \eta \delta^3(\vec{p} - \vec{p}_j)$ with $|\vec{p}| = k_f$.

In Fig. 3, the solid line shows the momentum dependence of the real single particle potential $U(p, k_{f0})$ at saturation density for momenta from zero up to the Fermi surface, $0 \leq p \leq k_{f0} = 272.7$ MeV. The dashed line in Fig. 3 represents the total single particle energy, $T_k(p) + U(p, k_{f0})$, i.e. the sum of single nucleon kinetic and potential energy. As required by the Hugenholtz-van-Hove theorem the dashed line ends at the Fermi surface $p = k_{f0} = 272.7$ MeV with the value $\bar{E}(k_{f0}) = -15.26$ MeV. The total single particle energy $T_k(p) + U(p, k_{f0})$ rises monotonically with the nucleon momentum p , as it should. Note however that there is no a priori guarantee for such a behavior in a perturbative calculation. The Hugenholtz-van-Hove theorem eq.(7) determines also the end point of the solid line in Fig. 3 as $U(k_{f0}, k_{f0}) = -54.0$ MeV. Since it starts with almost the same value $U(0, k_{f0}) = -53.2$ MeV at $p = 0$ the real single particle potential $U(p, k_{f0})$ cannot be a monotonically rising function of p in our calculation. As a matter of fact, one observes a downward bending of the real single particle potential $U(p, k_{f0})$ for nucleon momenta above $p = 180$ MeV. Such a behavior is also found in the calculation of ref.[3] based on the phenomenological Paris NN-potential, however, in much weaker form. The relativistic Dirac-Brueckner calculations of ref.[5] give, in contrast to this, single particle potentials which rise monotonically with the nucleon momentum p .

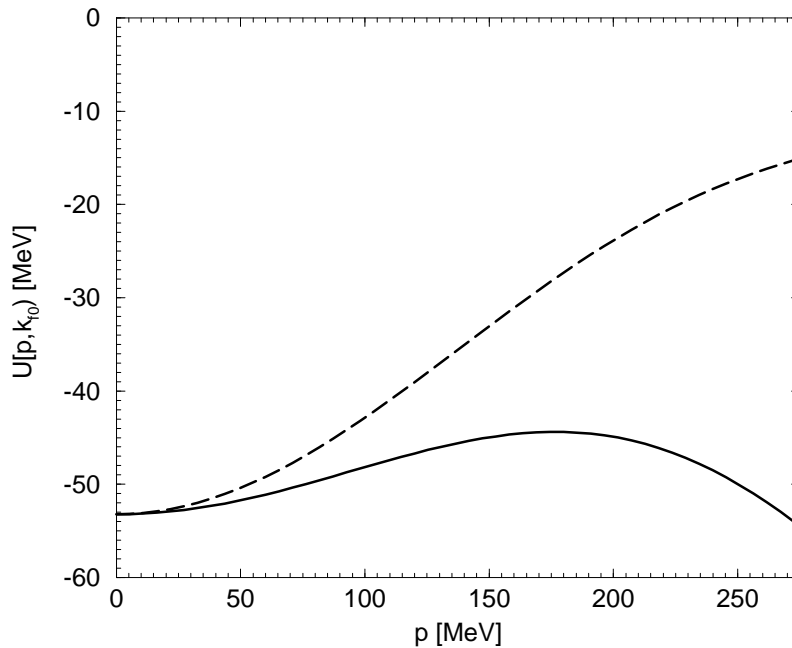


Fig. 3: The real part of the single particle potential $U(p, k_{f0})$ versus the nucleon momentum p at nuclear saturation density, $k_{f0} = 272.7$ MeV (solid line). The dashed line includes in addition the (relativistically improved) kinetic energy $T_k(p) = p^2/2M - p^4/8M^3$.

The momentum dependence of $U(p, k_{f0})$ translates into a variable effective nucleon mass $M^*(p)$ (the product of "k-mass" and "E-mass" divided by the free nucleon mass, according to

the nomenclature of ref.[1]) by the relation,

$$\frac{1}{M^*(p)} = \frac{1}{M} + \frac{1}{p} \frac{\partial U(p, k_{f0})}{\partial p}, \quad (18)$$

where $M = 939$ MeV is the (free) nucleon mass. Various many-body calculations [1, 3, 15] find that the variable effective nucleon mass $M^*(p)$ is reduced below $p \simeq 0.8k_{f0}$ and enhanced around the Fermi surface $p = k_{f0}$, typically by 20% on either side. The up- and downward bending of our real single particle potential $U(p, k_{f0})$ (solid line in Fig. 3) also produces such an effect, but the momentum dependence is too strong. On the other hand, according to the sum rule eq.(5), the detailed momentum dependence of the components of the real single particle potential $U_{2,3}(p, k_f)$ and therefore also that of the variable effective nucleon mass $M^*(p)$ is of almost no relevance for the nuclear matter equation of state. A more suitable quantity for comparison is the mean effective nucleon mass,

$$\frac{1}{\bar{M}^*} = \frac{1}{M} + \frac{2\Delta U}{k_{f0}^2}, \quad (19)$$

with ΔU the maximal change of the potential $U(p, k_{f0})$ in the momentum interval $0 \leq p \leq k_{f0}$. In the simple case that the real single particle potential grows quadratically with p , this \bar{M}^* agrees with the standard definition of the effective mass, eq.(18). By inspection of Fig. 3 one finds a maximal increase of our single particle potential $U(p, k_{f0})$ of $\Delta U = 8.8$ MeV. Via eq.(19) this shift ΔU translates into a mean effective nucleon mass of $\bar{M}^* = 0.82M$. This value is compatible with empirical effective nucleon mass $M_{emp}^* = (0.7 - 0.8)M$ derived from experimental data in the framework of non-relativistic shell or optical models [10, 11, 12].

The real single particle potential $U(p, k_f)$ has of course a smooth continuation above the Fermi surface, $p > k_f$. We will not consider $U(p, k_f)$ in this region, for two reasons. First, most of the integral representations for the contributions $U_{2,3}(p, k_f)$ given in section 3 do not hold anymore for $p > k_f$. Secondly, when going above the Fermi surface the relevant nucleon momentum soon becomes too large for the application of chiral perturbation theory (which should be restricted to $p \leq 300$ MeV), keeping in mind that this theory is an expansion in small external momenta such as p and k_f .

4 Imaginary part of the single particle potential

In this section, we discuss the imaginary part $W(p, k_f)$ of the single particle potential. For the reasons just mentioned, we will restrict ourselves to the momentum region below the Fermi surface, $0 \leq p \leq k_f$. In this region nucleon-hole states with restricted momentum, $0 \leq p \leq k_f$, can be prepared on top of the filled Fermi sea. Their total energy is $-T_k(p) - U(p, k_f) - iW(p, k_f)$, according to eq.(2). The (positive) imaginary single particle potential $W(p, k_f)$ accounts for the finite life time of a nucleon-hole state via $\tau_{hole}^{-1} = 2W(p, k_f)$. By on-shell NN-scattering processes the energy of a deeply bound hole-state gets redistributed among two hole-states closer to the Fermi surface and a nucleon state in the continuum (i.e. above the Fermi surface). Energy and momentum conservation as well as Pauli blocking limit the available phase space which vanishes for $p \rightarrow k_f$ as $(k_f - p)^2$ according to Luttinger's theorem [14]. Within the present three-loop chiral perturbation theory calculation of nuclear matter the contributions to the imaginary single particle potential $W(p, k_f)$ arise entirely from iterated one-pion exchange. As done in section 3 for the real part, we associate the contributions to $W(p, k_f)$ with the closed vacuum diagram (see Fig. 1) before opening of a nucleon line. Without going into further technical details, we

enumerate now the contributions to the components $W_n(p, k_f)$ and just indicate the type of iterated 1π -exchange diagram (Hartree or Fock) and the number of medium insertions n .

i) Hartree-diagram with two medium insertions:

$$\begin{aligned}
W_2(p, k_f) &= \frac{\pi g_A^4 M m_\pi^4}{(4\pi f_\pi)^4} \left\{ x^2 \left(\frac{x^2}{5} - 2u^2 + \frac{50}{3} \right) - 3u^4 - 34u^2 - 14 \right. \\
&\quad + \left(9 + 6u^2 + \frac{4u^3}{x} - 2x^2 \right) \ln[1 + (u+x)^2] + \left(9 + 6u^2 - \frac{4u^3}{x} - 2x^2 \right) \\
&\quad \left. \times \ln[1 + (u-x)^2] + \frac{1}{x} (7 + 15u^2 - 15x^2) \left[\arctan(u+x) - \arctan(u-x) \right] \right\} \quad (20)
\end{aligned}$$

with the abbreviations $u = k_f/m_\pi$ and $x = p/m_\pi$.

ii) Fock-diagram with two medium insertions:

$$\begin{aligned}
W_2(p, k_f) &= \frac{3\pi g_A^4 M m_\pi^4}{(4\pi f_\pi)^4} \left\{ \frac{u^4}{4} + \frac{u^2 x^2}{6} - \frac{x^4}{60} \right. \\
&\quad \left. - \left[\int_0^{(u-x)/2} d\xi 4\xi + \int_{(u-x)/2}^{(u+x)/2} d\xi \frac{1}{2x} (u^2 - (2\xi - x)^2) \right] \frac{1 + 4\xi^2}{1 + 2\xi^2} \ln(1 + 4\xi^2) \right\}. \quad (21)
\end{aligned}$$

iii) Hartree diagram with three medium insertions:

$$\begin{aligned}
W_3(p, k_f) &= \frac{3\pi g_A^4 M m_\pi^4}{(4\pi f_\pi)^4} \int_{-1}^1 dy \left\{ (u^2 - x^2 y^2) \left[\frac{2s^2 + s^4}{1 + s^2} - 2 \ln(1 + s^2) \right] + \frac{s^4 x^2 (y^2 - 1)}{1 + s^2} \right. \\
&\quad - \frac{3s^4}{2} + 10xy \left[\arctan s - s + \frac{s^3}{3} \right] + (3 + 2u^2 - 2x^2 y^2) \left[s^2 - \ln(1 + s^2) \right] \\
&\quad \left. + \int_0^u \frac{2\xi^2}{x} \theta(x - \xi|y|) \left[\frac{2\sigma^2 + \sigma^4}{1 + \sigma^2} - 2 \ln(1 + \sigma^2) \right] \right\}. \quad (22)
\end{aligned}$$

The auxiliary functions s and σ have been defined in eq.(12).

iv) Fock diagram with three medium insertions:

$$\begin{aligned}
W_3(p, k_f) &= \frac{3g_A^4 M m_\pi^4}{(4\pi f_\pi)^4} \int_{-1}^1 dy \left\{ \int_{-1}^1 dz \frac{\theta(1 - y^2 - z^2)}{4\sqrt{1 - y^2 - z^2}} \left[s^2 - \ln(1 + s^2) \right] \left[\ln(1 + t^2) - t^2 \right] \right. \\
&\quad \left. + \int_0^u d\xi \frac{\pi \xi^2}{x} \theta(x - \xi|y|) \left[\ln(1 + \sigma^2) - \sigma^2 \right] \left(1 - \frac{1}{R} \right) \right\}. \quad (23)
\end{aligned}$$

The auxiliary functions t and R have been defined in eq.(15).

v) Hartree diagram with four medium insertions:

$$\begin{aligned}
W_4(p, k_f) &= \frac{6\pi g_A^4 M m_\pi^4}{(4\pi f_\pi)^4} \left\{ \frac{7}{2} - \frac{8x^2}{3} + \frac{8x^4}{15} - 3 \ln(1 + 4x^2) + \left(5x - \frac{7}{4x} \right) \arctan 2x \right. \\
&\quad + \int_{-1}^1 dy \left[10xy \left[s - \frac{s^3}{3} - \arctan s \right] + (3 + 2u^2 - 2x^2 y^2) \left[\ln(1 + s^2) - s^2 \right] \right. \\
&\quad \left. \left. + \frac{3s^4}{2} + \frac{s^4 x^2 (1 - y^2)}{1 + s^2} \right] \right\}, \quad (24)
\end{aligned}$$

vi) Fock diagram with four medium insertions:

$$\begin{aligned}
W_4(p, k_f) &= \frac{3\pi g_A^4 M m_\pi^4}{(4\pi f_\pi)^4} \int_0^u d\xi \int_{-1}^1 dy \frac{\xi^2}{x} \left(1 - \frac{1}{R} \right) \left\{ \theta(x - \xi|y|) \theta(\xi - x) \right. \\
&\quad \left. \times \left[\sigma^2 - \ln(1 + \sigma^2) \right] + \theta(x - \xi) \left[\sigma_x^2 - \ln(1 + \sigma_x^2) \right] \right\}, \quad (25)
\end{aligned}$$

with a new auxiliary function

$$\sigma_x = \xi y + \sqrt{u^2 - x^2 + \xi^2 y^2}. \quad (26)$$

The total sum of these six contributions eqs.(20-25) evaluated at zero nucleon momentum ($p = 0$) can even be written as a closed form expression,

$$W(0, k_f) = \frac{3\pi g_A^4 M m_\pi^4}{(4\pi f_\pi)^4} \left\{ \frac{u^4}{2} - 4u^2 - \frac{2u^2}{1+u^2} + \frac{\pi^2}{12} + \text{Li}_2(-1-u^2) \right. \\ \left. + \left[6 + u^2 + \ln(2+u^2) - \frac{1}{2} \ln(1+u^2) \right] \ln(1+u^2) \right\}, \quad (27)$$

with $u = k_f/m_\pi$ and $\text{Li}_2(-a^{-1}) = \int_0^1 d\zeta (\zeta + a)^{-1} \ln \zeta$ denotes the conventional dilogarithmic function. Note that eq.(27) determines the half width of a nucleon-hole state at the bottom of the Fermi sea. The density dependence of $W(0, k_f)$ in eq.(27) goes approximately as $\rho^{4/3}$ since the first term, $u^4/2$, in the curly bracket dominates. This is in fact also the only term which survives in the chiral limit $m_\pi = 0$.

4.1 Results

Evidently, the results for the imaginary single particle potential $W(0, k_f)$ are completely parameterfree (to the order we are working here). At saturation density $\rho_0 = 0.178 \text{ fm}^{-3}$ (corresponding to $k_{f0} = 272.7 \text{ MeV}$) we find from eq.(27) a half width for a nucleon-hole state at the bottom of the Fermi sea of $W(0, k_f) = 29.7 \text{ MeV}$. This is not far from the value $W(0, k_f) \simeq 40 \text{ MeV}$ obtained in the self-consistent Brueckner calculation of ref.[3] using the phenomenological Paris NN-potential. On the other hand the calculation of ref.[15] employing the Gogny D1 effective interaction finds about half of the value of ref.[3], namely $W(0, k_f) \simeq 20 \text{ MeV}$. Taking the results of these two calculations as a reasonable benchmark our prediction for the imaginary single particle potential at zero-momentum, $W(0, k_f) = 29.7 \text{ MeV}$, can be considered as fairly realistic.

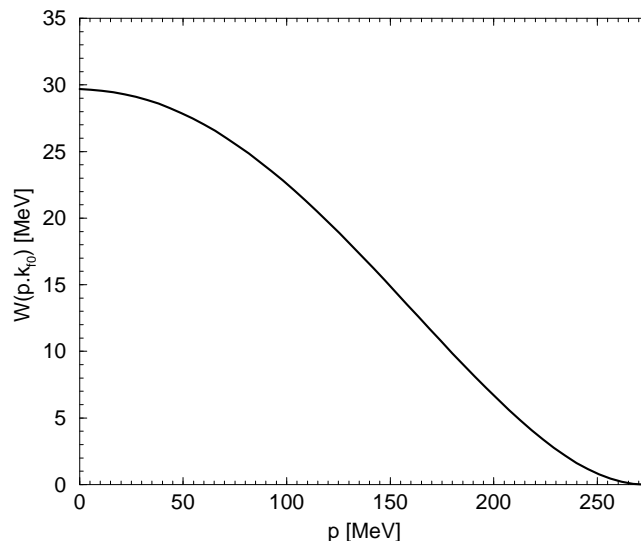


Fig. 4: The imaginary part of the single particle potential $W(p, k_{f0})$ versus the nucleon momentum p at nuclear matter saturation density, $k_{f0} = 272.7 \text{ MeV}$.

In Fig. 4, we show the momentum dependence of the imaginary part of the single particle potential $W(p, k_{f0})$ at nuclear matter saturation density, $k_{f0} = 272.7$ MeV. As a consequence of the decreasing phase space available for the redistribution of a nucleon-hole state's energy the curve in Fig. 4 drops with momentum p and $W(p, k_{f0})$ reaches zero at the Fermi surface $p = k_{f0}$. From the formulas eq.(20-26) given above one can actually proof that both the value $W(k_f, k_f)$ and the slope $[\partial W(p, k_f)/\partial p]_{p=k_f}$ vanish identically at the Fermi surface $p = k_f$. This is even separately true for the contributions of the iterated 1π -exchange Hartree- and Fock-diagram. Luttinger's theorem [14] is therefore satisfied in our perturbative calculation. The imaginary single particle potential grows quadratically near the Fermi surface,

$$W(p, k_f) = C(k_f) \cdot (p - k_f)^2 + \dots, \quad (28)$$

with $C(k_f)$ a density dependent curvature coefficient. The quantity $C(k_f)$ is useful in order to characterize the damping of the single particle motion of valence nucleons in nuclei [2]. In Fig. 5, we show the dependence of the curvature coefficient $C(k_f)$ (given in units of GeV^{-1}) on the density for $\rho \leq 0.4 \text{ fm}^{-3}$. One observes an approximate $\rho^{2/3}$ -dependence of $C(k_f)$. This behavior can be easily understood when taking the chiral limit $m_\pi = 0$. In that case the proportionality $C(k_f) \sim k_f^2$ becomes a simple consequence of (mass) dimension counting.

Finally, we note that the zero sum rule eq.(6) for the two-, three- and four-body components of the imaginary single particle potential $W_{2,3,4}(p, k_f)$ holds with high numerical accuracy separately for the iterated 1π -exchange Hartree- and Fock-diagram. This serves as an important check on our calculation.

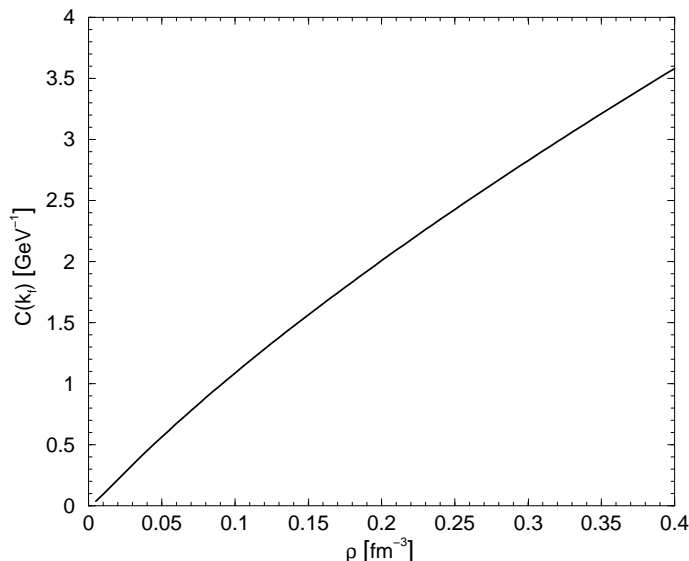


Fig. 5: The curvature coefficient $C(k_f)$ of the imaginary part of the single particle potential $W(p, k_f)$ versus the nucleon density $\rho = 2k_f^3/3\pi^2$.

5 Concluding Remarks

In this paper, we have continued the systematic treatment of the nuclear matter many-body problem in the framework of chiral perturbation theory by calculating the (complex-valued) single particle potential or nuclear mean field. From the good results of our previous paper [6] and the present work one can indeed conclude that perturbative chiral pion-nucleon dynamics

is able to produce nuclear binding and saturation (including its isospin dependence) as well as realistic in-medium single particle properties (including the average nuclear mean field). Most surprisingly, all this can be achieved with only one adjustable parameter, namely a single cut-off scale $\Lambda \simeq 0.65 \text{ GeV}$ which represents short distance NN-dynamics.

Our approach to the nuclear matter problem is in many respects different from most other commonly used ones. First, we do not start from a so-called realistic NN-potential (which fits deuteron properties and NN-phase shifts), but we use instead well-founded chiral pion-nucleon dynamics. From that we calculate analytically in-medium multi-loop diagrams up to a certain order in a small momentum expansion. This "inward-bound" method starts from large distances (small Fermi momentum k_f) and systematically generates the pion-induced correlations between nucleons as they develop with decreasing distance (increasing k_f) down to the average NN-distance in nuclear matter, $\bar{d} \simeq 1.8 \text{ fm}$, which is just slightly larger than the pion Compton wave length $m_\pi^{-1} = 1.46 \text{ fm}$.

Of course, open questions concerning the role of yet higher orders in the chiral expansion remain and should be explored.

References

- [1] C. Mahaux and R. Sartor, *Adv. Nucl. Phys.* **20** (1991) 1; and refs. therein.
- [2] J.P. Jeukenne, A. Lejeune and C. Mahaux, *Phys. Reports* **25** (1976) 83.
- [3] P. Grange, J.P. Cugnon and A. Lejeune, *Nucl. Phys.* **A473** (1987) 365.
- [4] B. ter Haar and R. Malfliet, *Phys. Reports* **149** (1987) 207.
- [5] G.Q. Li, R. Machleidt and R. Brockmann, *Phys. Rev.* **C45** (1992) 2782.
- [6] N. Kaiser, S. Fritsch and W. Weise, *Nucl. Phys.* **A** (2001) in print; nucl-th/0105057.
- [7] G.L. Thomas and E.J. Burge, *Nucl. Phys.* **A128** (1969) 545; W.T.H van Oers, *Phys. Rev.* **C3** (1971) 1550.
- [8] P.E. Hodgson, *Rep. Prog. Phys.* **47** (1984) 613.
- [9] A. Bohr and B.R. Mottelson, *Nuclear Structure, Vol.I*, Benjamin (1969).
- [10] C.H. Johnson, D.J. Horen and C. Mahaux, *Phys. Rev.* **C36** (1987) 2252.
- [11] M. Jaminon and C. Mahaux, *Phys. Rev.* **C40** (1989) 354.
- [12] M. Brack, C. Guet and H.B. Hakansson, *Phys. Reports* **123** (1985) 275.
- [13] N.M. Hugenholtz and L. Van Hove, *Physica* **24** (1958) 363.
- [14] J.M. Luttinger, *Phys. Rev.* **121** (1961) 942.
- [15] R.W. Hasse and P. Schuck, *Nucl. Phys.* **A445** (1985) 205.